J|A|C|S ARTICLES

Published on Web 04/07/2009

Enhancement of Field Emission Transport by Molecular Tilt Configuration in Metal−Molecule−Metal Junctions

Gunuk Wang, Tae-Wook Kim, Gunho Jo, and Takhee Lee*

Department of Materials Science and Engineering, Gwangju Institute of Science and Technology, Gwangju 500-712, Korea

Received January 31, 2009; E-mail: tlee@gist.ac.kr

Abstract: We studied the molecular configuration-dependent charge transport of alkyl metal−molecule−metal junctions using conducting atomic force microscopy (CAFM). The inflection point (or transition voltage V_T) on the plot of $\ln(I/V^2)$ versus $1/V$ shifted to a lower voltage with increasing CAFM tip-loading force and decreasing molecular length. Our results indicate that the reduction of gap distance by molecular tilt configuration enhances the transition of the electronic transport mechanism from direct tunneling to field emission transport through molecules. The obtained results are consistent with a barrier height decrease, as affected by the enhancement of the intermolecular chain-to-chain tunneling as molecular tilt, predicted by a multibarrier tunneling model.

1. Introduction

Controlling the charge transport characteristics through molecules between metal electrodes is important to understanding basic conduction mechanism and realizing potential device applications of molecular electronic systems.[1−5] The charge transport characteristics in molecular junctions are influenced by molecular structure, metal−molecule contact, conformational effect, and alignment of molecular orbitals with the Fermi levels of the electrodes.[3−11] For example, there are noticeable differences between alkyl and conjugated molecules in terms of the conductance of charge transport.[3] The small highest occupied molecular orbital (HOMO)−lowest unoccupied molecular orbital (LUMO) gap for π-bonded molecules (3−5 eV),[3,12] as compared to that of alkyl molecules (∼8 eV),[3,13] explains the greater conductance through the former. Recently, Beebe et al. demonstrated that metal−molecule−metal junctions formed with π-conjugated thiols having small HOMO−LUMO gaps exhibit a current−voltage behavior that is consistent with a transition from direct tunneling (DT) to field emission (so-called Fowler−Nordheim (FN) tunneling).[12] Yet no such transition was observed for the case of alkyl molecular junctions at a moderate voltage range (<∼1 V).[12−14] In addition to the energy gap differences caused by the molecular structure (π-bond vs σ-bond), charge transport through molecules can also be strongly influenced by their molecular geometrical structures or configurations. For example, the conductance in a biphenyl molecular system, which has two benzene rings, decreases with increasing twist angle between the two rings.[8] Even in the simple σ-bond alkyl molecules, conductance and inelastic tunneling can also be significantly influenced by the molecular tilt configuration.[15] However, a comprehensive analysis of the changes in the conduction mechanism for different configurations of alkyl molecules has not been thoroughly completed. Therefore, it is interesting to investigate molecular-configuration-dependent charge transport to understand the intrinsic mechanism for the conductance changes affected by molecular configuration.

In this study, we investigated the effect of molecular configuration on the electronic transport in alkyl metal−molecule−metal junctions, wherein the molecular configuration was controlled by a conducting atomic force microscopy (CAFM) tip. In CAFM, the tip-loading force is directly applied to the molecules so as to change the molecular tilt configuration. Our results indicate that the reduction of gap distance by molecular tilt configuration enhances the transition of the electronic

(1) Reed, M. A.; Zhou, C.; Muller, C. J.; Burgin, T. P.; Tour, J. M. *Science* **1997**, *278*, 252.
(2) Nitzan, A.; Ratner, M. A. *Science* **2003**, *300*, 1384.
(3) Salomon, A.; Cahen, D.; Lindsay, S.; Tomfohr, J.; Engelkes, V. B.; Frisbie, C. D. *Adv. Mater.* **2003**, *15*, 1881.
(4) Troisi, A.; Beebe, J. M.; Picraux, L. B.; van Zee, R. D.; Stewart, D. R.; Ratner, M. A.; Kushmerick, J. G. *Proc. Natl. Acad. Sci. U.S.A.* **2007**, *104*, 14255.
(5) Green, J. E.; Choi, J. W.; Boukai, A.; Bunimovich, Y.; Johnston-Halperin, E.; DeIonno, E.; Luo, Y.; Sheriff, B. A.; Xu, K.; Shin, Y. S.; Tseng, H.-R.; Stoddart, J. F.; Heath, J. R. *Nature (London)* **2007**, *445*, 414.
(6) Dulić, D.; van der Molen, S. J.; Kudernac, T.; Jonkman, H. T.; de Jong, J. J. D.; Bowden, T. N.; van Esch, J.; Feringa, B. L.; van Wees, B. J. *Phys. Rev. Lett.* **2003**, *91*, 207402.
(7) Kim, B.; Beebe, J. M.; Jun, Y.; Zhu, X.-Y.; Frisbie, C. D. *J. Am. Chem. Soc.* **2006**, *128*, 4970.
(8) Venkataraman, L.; Klare, J. E.; Nuckolls, C.; Hybertsen, M. S.; Steigerwald, M. L. *Nature (London)* **2006**, *442*, 904.
(9) Venkataraman, L.; Park, Y. S.; Whalley, A. C.; Nuckolls, C.; Hybertsen, M. S.; Steigerwald, M. L. *Nano Lett.* **2007**, *7*, 502.
(10) Kumar, A. S.; Ye, T.; Takami, T.; Yu, B.-C.; Flatt, A. K.; Tour, J. M.; Weiss, P. S. *Nano Lett.* **2008**, *8*, 1644.
(11) Kronemeijer, A. J.; Akkerman, H. B.; Kudernac, T.; van Wees, B. J.; Feringa, L.; Blom, P. W. M.; de Boer, B. *Adv. Mater.* **2008**, *20*, 1467.
(12) Beebe, J. M.; Kim, B. S.; Gadzuk, J. W.; Frisbie, C. D.; Kushmerick, J. G. *Phys. Rev. Lett.* **2006**, *97*, 026801.
(13) Wang, W.; Lee, T.; Reed, M. A. *Phys. Rev. B* **2003**, *68*, 035416.
(14) Beebe, J. M.; Kim, B. S.; Frisbie, C. D.; Kushmerick, J. G. *ACS Nano* **2008**, *2*, 827.
(15) (a) Slowinski, K.; Chamberlain, R. V.; Miller, C. J.; Majda, M. *J. Am. Chem. Soc.* **1997**, *119*, 11910. (b) Yamamoto, H.; Waldeck, D. H. *J. Phys. Chem. B* **2002**, *106*, 7469. (c) Wold, D. J.; Frisbie, C. D. *J. Am. Chem. Soc.* **2001**, *123*, 5549. (d) Song, H.; Lee, H.; Lee, T. *J. Am. Chem. Soc.* **2007**, *129*, 3806. (e) Okabayashi; Konda, N. Y.; Komeda, T. *Phys. Rev. Lett.* **2008**, *100*, 217801.

10.1021/ja900773h CCC: $40.75

Scheme 1. Schematic of a Molecular Junction Using the CAFM Method[a]

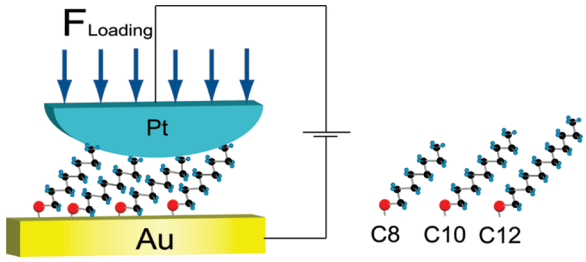

[a] C8, C10, and C12 molecular structures are shown.

transport mechanism from DT to field emission transport through molecules. We also compared the experimental results to a theoretical calculation based on a multibarrier tunneling (MBT) model that assumes an intermolecular chain-to-chain transport mechanism.[16,17]

2. Experimental Section

Three different ~5 mM alkyl solutions were prepared by adding ~10 μL of alkanethiol molecules to ~10 mL of anhydrous ethanol (Aldrich Chem. Co). The samples were left in the solution for 24−48 h to allow self-assembled monolayer (SAM) to assemble on Au surface (Au (500 Å)/Ti (50 Å)/SiO_2 (3000 Å)/Si) in a nitrogen-filled glovebox with oxygen of less than ~10 ppm. Alkanethiols of various molecular lengths, octanethiol ($CH_3(CH_2)_7SH$, denoted as C8 for the number of alkyl units), decanethiol ($CH_3(CH_2)_9SH$, C10), and dodecanethiol ($CH_3(CH_2)_{11}SH$, C12), were used to form the active molecular components. Before use, each sample was rinsed with a few milliliters of ethanol and gently blown dry in a stream of N_2. Experiments were performed using a commercially available AFM system (PSIA, XE-100 model) with CAFM tips that were made from Pt (10 nm)/Ti (20 nm)-coated conventional AFM tips. The tip radius was determined as 90 ± 40 nm from scanning electron microscopic images (Figure S1 in the Supporting Information). Two terminal DC current−voltage ($I-V$) measurements were performed using a semiconductor parameter analyzer (HP4145B). Using CAFM, the $I-V$ characteristics of alkanethiol SAMs between the CAFM tip (Pt tip) and the Au surface (grounded) were measured while the molecular compression (or molecular tilt configuration) was controlled by applying a variable tip-loading force to the molecules, as schematically illustrated in Scheme 1. All electrical measurements were carried out inside a covered AFM chamber in ambient through which nitrogen gas was being passed to minimize the formation of a contamination layer on SAM surface and to keep constant humidity (relative humidity 25−30%). Typically, we performed the $I-V$ measurements on roughly 15−20 different junction positions and repeated the measurements several times (at least 5−10 times) on each particular junction position to obtain one data point and its error bar. When the CAFM $I-V$ measurements frequently produced an electric open or a short, we changed the CAFM tips or sample positions.

2.1. Theoretical Basis. 2.1.1. Through-Bond and Through-Space Tunneling. The metal−molecule−metal junctions are completed by placing a CAFM tip in stationary point contact with alkanethiol SAMs under a controlled tip-loading force that defines the contact angle with the molecules.[15c,d] Under a force-loaded tip contact, the molecular tilt angle with respect to the substrate normal is expected to increase (Table S1 and Figure S5 in the Supporting Information).[15,18] Several authors have suggested the existence of an ordered tilted-chain phase of alkanethiol SAMs on Au(111) as a function of the loading effect applied by the tip.[18] Most of the deformation under a tip-loading force leads to additional tilting of the molecules.[19,20] Thus, in terms of molecular geometry, we assume that an increase in tip-loading force tilts the alkanethiol molecules without seriously collapsing their molecular conformation, even though gauche and other defect-related deformations might cause a small change in the overall charge transfer characteristics.[15a,b,d]

As the molecular tilt angle increases as a function of tip-loading force, the vertical distance (i.e., film thickness d_t) between the top and bottom electrodes is reduced by δ (Figure 1a). Herein, the chain-to-chain tunneling (or "through-space" tunneling) becomes significant in addition to the already existing "through-bond" tunneling in the overall charge transport,[15a,b,d] as schematically illustrated in Figure 1a. In the case of through-bond tunneling, charge flows along the σ-bond in the backbone of the alkyl chains. This process is, therefore, independent of molecular tilt angle. In contrast, chain-to-chain tunneling involves lateral hops via intermolecular couplings between neighboring alkyl chains, which depends on the molecular tilt configuration by compression.[15a,b,d] The tunneling distance in the chain-to-chain tunneling pathway is $d - d_{cc} \tan\theta + d_{cc}$ (d is the molecular length, and d_{cc} is the molecular chain-to-chain distance, ~4.97 Å[15d,21]), which is shorter than that for the through-bond tunneling pathway (Figure 1a). The barrier width in chain-to-chain tunneling can be reduced by molecular tilting angle (θ), which is determined by compression length (δ).[22,23] Note that this barrier thinning by compression can affect the chain-to-chain tunneling and thus the total charge transfer in the molecular junction, resulting in the enhancement of field emission by the enhancement of electric field. The compression, δ, and tilt angle, θ, can be estimated using mechanical contact theory[22,23] (see the Supporting Information).

2.2. Multibarrier Tunneling Model. Figure 1b schematically depicts the proposed multibarrier tunneling (MBT) model used in this study to describe the charge transport in the molecular junction.[16] The enhancement of field emission as a function of tip-loading force and molecular tilt configuration by compression can be explained by the configuration-dependent barrier height, $\Phi_B(\theta)$. This means that the barrier thinning by tip loading compression (molecular tilt) appears as a barrier lowering effect, that is, enhancement of field emission. The barrier height, $\Phi_B(\theta)$,

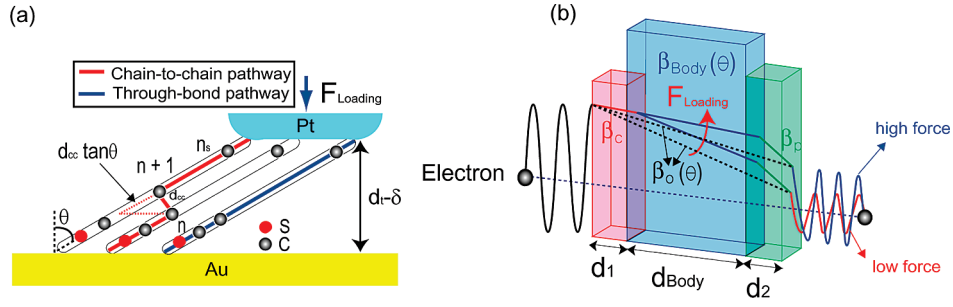

Figure 1. (a) Schematic illustrating tunneling pathways through alkanethiol. (b) Schematic of the multibarrier tunneling (MBT) model for an alkanethiol junction.

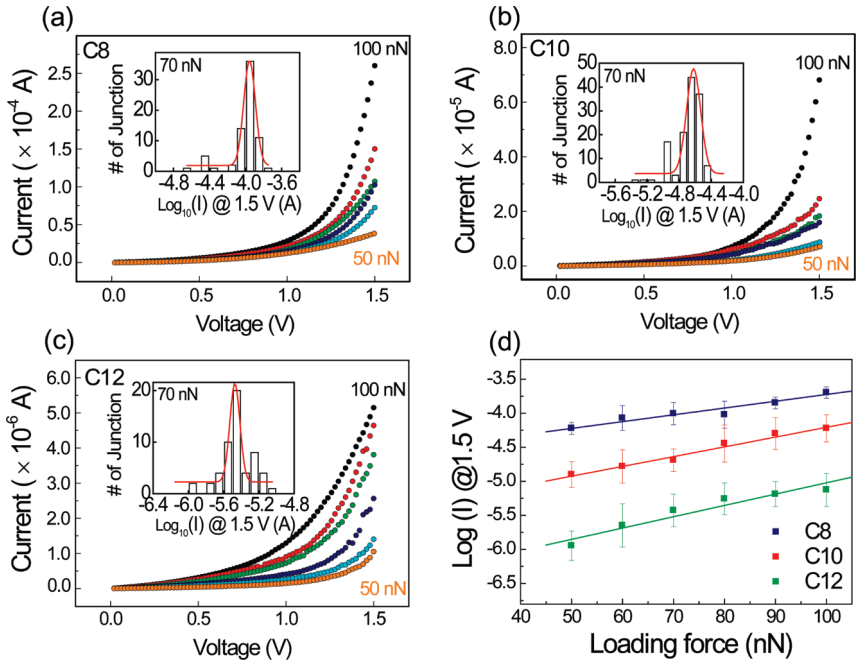

Figure 2. (a) Force-dependent $I-V$ data for a C8 SAM when the tip-loading force is varied from 50 to 100 nN at 10 nN increments. The inset is the statistical histogram of currents at 1.5 V, obtained from 64 $I-V$ measurements on the C8 SAM at a fixed loading force of 70 nN with a fit curve found by a Gaussian function. (b) Data for C10. (c) Data for C12. (d) Force-dependent log(I) at 1.5 V for C8, C10, and C12 molecular junctions.

can be expressed with the overall decay coefficient, $\beta_o(\theta)$ (or $\beta_{Body}(\theta)$), in the MBT model[16,17] (Figure 1b):

$$\Phi_B(\theta) = \left(\frac{\hbar}{2(2m)^{1/2}\alpha}\beta_o(\theta)\right)^2 = \left(\frac{\hbar}{2(2m)^{1/2}\alpha}\frac{\beta_C d_1 + \beta_{Body}(\theta) d_{Body} + \beta_P d_2}{d_1 + d_{Body} + d_2}\right)^2 \quad (1)$$

where m is the electron mass, α accounts for the effective mass of the tunneling electrons through a barrier, $\beta_{C(P)}$ is the chemisorbed (physisorbed) contact decay coefficient component corresponding to the chemisorbed (physisorbed) contact width d_1 (d_2) and denoted by a red line (green line), and $\beta_{Body}(\theta)$ is the molecular body decay coefficient corresponding to the molecular-chain width d_{Body}, as described in Figure 1b. Here, the chemisorbed and physisorbed contacts of molecules are formed with the Au substrate and Pt CAFM tip, respectively. The contact decay coefficients, $\beta_{C(P)}$, and molecular width (d_1, d_2, and d_{Body}) for C8, C10, and C12 are reported elsewhere.[13,16,17] As the molecular tilt angle is increased by increasing the tip-loading force, the electron tunneling probability through the molecular junction is increased due to the additional chain-to-chain tunneling pathway and intermolecular charge transfer, which is strongly dependent on the molecular tilt configuration by compression (barrier thinning). This leads to a reduction of $\beta_{Body}(\theta)$. The $\beta_{Body}(\theta)$ can be determined from the total tunneling current by considering both contributions from the through-bond and through-space tunneling as:[15a,b,d]

$$I = I_o e^{-\beta_{Body} d_{Body}} + I_o \sum_{N=1}^{d_{Body}\cos\theta/d_{cc}} \frac{(n_s-1)!}{(n_s-(1+N))!\,N!} e^{-\beta_{Body}(d_{Body}-Nd_{cc}\tan\theta)} e^{-\beta_{ts} N d_{cc}} = I_o e^{-\beta_{Body}(\theta) d_{Body}} \quad (2)$$

where I_o is a current coefficient, N is the number of intermolecular hops (we assumed $N = 1$), and the statistical factor n_s accounts for the increased number of pathways caused by the influence of intermolecular charge transfer and is assumed to be the same as the number of carbon atoms in the alkanethiol.[15a,b,d] Here, β_{Body} (=0.91 Å) and β_{ts} (=1.31 Å) are tunneling decay factors ($\theta = \sim 30°$) for molecular-chain body and through-space tunneling, respectively.[15a,d] From the model, we can calculate the barrier height, $\Phi_B(\theta)$, from eq 1 using the fit parameter α ($0 < \alpha \leq 1$) and by reducing $\beta_{Body}(\theta)$ using the enhancement of through-space tunneling (second term in eq 2) with molecular tilt configuration affected by a variety of CAFM tip-loading forces and different alkanethiol lengths.

3. Results and Discussion

Figure 2a–c shows a series of force-dependent representative $I-V$ characteristics measured from C8, C10, and C12 SAMs while the tip-loading force was varied from 50 to 100 nN at 10 nN increments, respectively. The insets in these figures display the statistical histograms of currents at 1.5 V with a logarithmic scale for C8, C10, and C12 SAMs at a fixed loading force of

(16) Wang, G.; Kim, T.-W.; Lee, H.; Lee, T. *Phys. Rev. B* **2007**, *76*, 205320.
(17) Wang, G.; Kim, T.-W.; Jang, Y. H.; Lee, T. *J. Phys. Chem. C* **2008**, *112*, 13010.
(18) (a) Barrena, E.; Ocal, C.; Salmeron, M. *J. Chem. Phys.* **2000**, *113*, 2413. (b) Barrena, E.; Ocal, C.; Salmeron, M. *J. Chem. Phys.* **2001**, *114*, 4210.
(19) Siepmann, J. I.; Mcdonald, I. R. *Phys. Rev. Lett.* **1993**, *70*, 453.
(20) Cui, X. D.; Zarate, X.; Tomfohr, J.; Sankey, O. F.; Primak, A.; Moore, A. L.; Moore, T. A.; Gust, D.; Harris, G.; Lindsay, S. M. *Nanotechnology* **2002**, *13*, 5.
(21) Ulman, A. *An Introduction to Ultrathin Organic Films from Langmuir-Blodgett to Self-Assembly*; Academic Press: Boston, 1991.
(22) Johnson, K. L. *Contact Mechanics*; Cambridge University Press: New York, 1985; pp 104–106.
(23) The contact separation ($d \cos\theta = d_t - \delta$) is shortened when the tip makes contact with a SAM by the applied loading force. We used a spring model, an elastic foundation model,[22] to estimate the reduced distance $\delta = a^2/2R$ induced by the high tip-loading force, where a (determined by the Hertzian elastic contact model[15c,22] is the radius of the contact area, and R is the radius of the tip ($R \approx 90$ nm)). The tilt angle θ of molecules under the tip contact can be geometrically calculated as $\cos^{-1}[(d_t-\delta)/d]$.[15d]

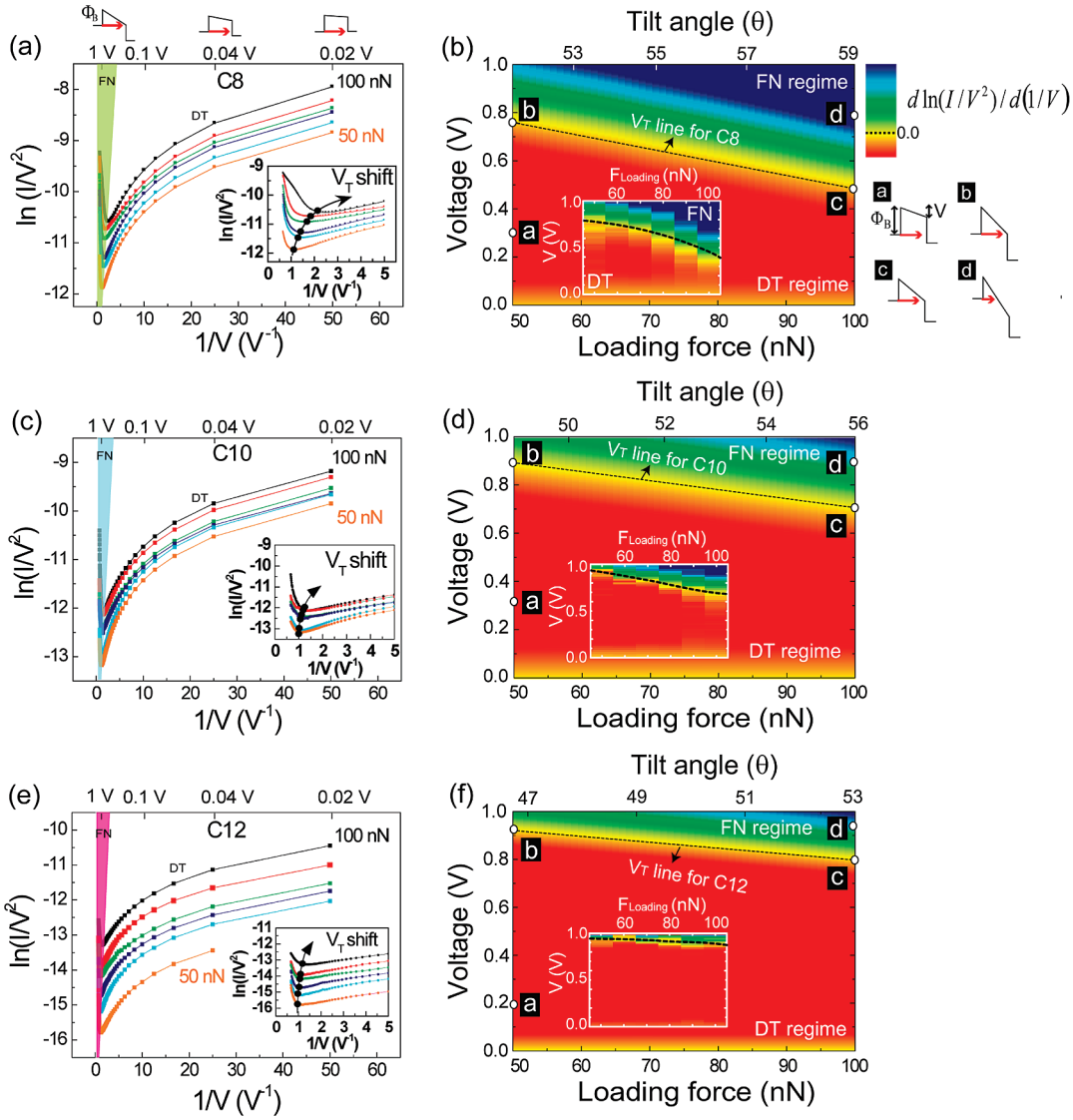

Figure 3. Representative plots of $\ln(I/V^2)$ versus $1/V$ for (a) C8, (c) C10, and (e) C12 with various tip-loading forces (50−100 nN). Insets show the transition voltage (V_T) from DT to FN tunneling shifts to a lower bias when the tip-loading force is increased. Contour plots of the calculated data of normalized $d(\ln(I/V^2))/d(1/V)$ for (b) C8, (d) C10, and (f) C12 SAM as a function of applied voltage under various tip-loading forces (from 50 to 100 nN, at 1 nN increments) and molecular tilt angle (see text). The solid V_T line from point **b** to **c** corresponds to the transition from DT to FN tunneling. The inset figures show contour plots of experimental data of $d(\ln(I/V^2))/d(1/V)$ as a function of applied voltage under various tip-loading forces (from 50 to 100 nN at 10 nN increments).

70 nN, with fit curves found using Gaussian functions. Figure 2d summarizes statistical force-dependent log(I) measured at 1.5 V with C8, C10, and C12 molecular junctions under various tip-loading forces (from 50 to 100 nN, 10 nN step). The current through the junction increases with molecular tilting, as a function of an increasing applied tip-loading force, due to the enhancement of chain-to-chain tunneling, in addition to the already existing through-bond tunneling. From Figure 2d, the current for the shorter molecule was observed to be larger, which was consistent with the dependence of the tunneling current on the gap distance.[3,13−17] The error bars in Figure 2d were determined as the standard deviation from statistical measurements. Note that the tips with different radius of curvature can result in the variation in the current levels and transition voltage under the same loading force (see Figures S3 and S4 in the Supporting Information).

Figure 3 shows the transition of DT to field emission transport for C8, C10, and C12 molecular junctions under various tip-loading forces. A plot of $\ln(I/V^2)$ versus $1/V$ exhibits logarithmic growth when the applied bias is less than the barrier height ($V < \Phi_B$) in the DT regime, whereas this plot exhibits a linear decay when the applied bias is higher than the barrier height ($V \geq \Phi_B$) in the field emission transport regime.[12] The transition from DT to field emission accompanies a change of the barrier shape from trapezoidal to triangular and appears as an inflection in the plot of $\ln(I/V^2)$ versus $1/V$, as shown in Figure 3a, c, and e. Thus, the transition voltage V_T corresponds to the barrier height Φ_B. Figure 3a shows a plot of $\ln(I/V^2)$ versus $1/V$ of C8 molecular junction under various tip-loading forces (50−100 nN). A zoomed-in plot near the transition voltage is shown in the inset of Figure 3a. The line with an arrow in this inset denotes the bias required for the transition from DT to field emission. This phenomenon was consistently observed for other molecules (C10 and C12 SAMs), as shown in Figure 3c and e. The key phenomenon observed in Figure 3a, c, and e is that the inflection point, that is, the transition voltage V_T, shifted to

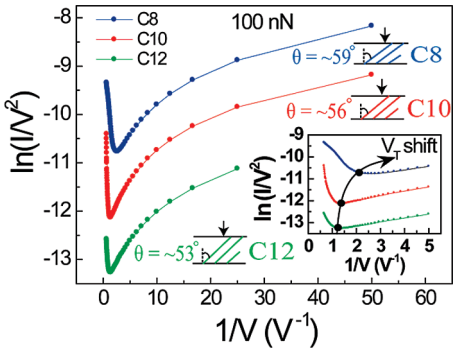

Figure 4. Representative plot of $\ln(I/V^2)$ versus $1/V$ for C8, C10, and C12 at a fixed tip-loading force of 100 nN. The tilt angle was estimated using contact mechanics models[22,23] (see Table S1 in the Supporting Information). Insets show the transition voltage (V_T) from DT to field emission occurs at a lower bias for shorter molecules.

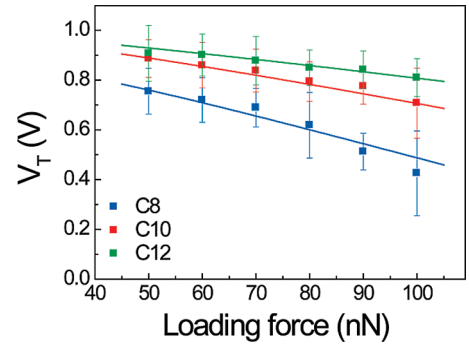

Figure 5. Experimental V_T versus tip-loading force for C8, C10, and C12 molecular junctions with calculated values (solid lines) from the MBT model.

the lower bias as the tip-loading force was increased. This is because the electric field was enhanced by the reduction of vertical gap by molecular tilt configuration while the tip-loading force was increased. It has been reported that molecules become more tilted with increasing tip-loading force, resulting in a significant contribution of the molecular chain-to-chain transport (so-called through-space transport) in the overall conduction in molecular junctions.[15d] The shift of transition voltage to the lower bias in Figure 3 indicates the reduction of the barrier height Φ_B for the molecular junction, that is, enhancement of field emission. Note that under lower tip-loading forces, we did not observe the transition voltage from DT to field emission (see Figure S2 in the Supporting Information), which is consistent with previous studies.[14]

Figure 3b shows a contour plot of the calculated data of normalized $d(\ln(I/V^2))/d(1/V)$ for a C8 SAM as a function of applied voltage (from 0 to 1 V) under various tip-loading forces (from 50 to 100 nN, at 1 nN increments) and molecular tilt angles using eqs 1 and 2. The dotted line from point b to point c denotes the V_T line, which corresponds to $d(\ln(I/V^2))/d(1/V) = 0$. Along this line, the applied voltage V is identical to the molecular barrier height, which indicates the onset of field emission (Fowler−Nordheim (FN) tunneling). In Figure 3b, the region below the V_T line is the DT regime, and the region above the V_T line is the FN tunneling regime. For example, points **a** and **d** are in the DT and FN tunneling regime, respectively. It is clear that the transition from DT to FN tunneling occurs at a lower bias with increasing tip-loading force, due to the enhancement of field emission by the molecular tilt configuration. The inset in Figure 3b shows a contour plot of the experimental data of $d(\ln(I/V^2))/d(1/V)$ for a C8 SAM as a function of applied voltage (from 0 to 1 V) under various tip-loading forces (from 50 to 100 nN, at 10 nN steps). The dotted line in this inset denotes the V_T line. This phenomenon was consistently observed for other molecules (C10 and C12 SAMs), as shown in Figure 3d and f. The experimental V_T values for C8, C10, and C12 were reduced from 0.76 ± 0.09 to 0.43 ± 0.17 V, from 0.89 ± 0.08 to 0.71 ± 0.14 V, and from 0.91 ± 0.11 to 0.81 ± 0.08 V when the tip-loading force was increased from 50 to 100 nN, respectively, which agrees well with calculated results (the calculated V_T values for C8, C10, and C12 were found to change from 0.76 to 0.49 V, from 0.89 to 0.71 V, and from 0.93 to 0.81 V under the same change in loading force, respectively).

Figure 4 shows the representative $\ln(I/V^2)$ versus $1/V$ at a fixed tip-loading force of 100 nN for C8, C10, and C12 molecular junctions. As the molecular length decreases, the inflection point (transition voltage) occurs at a lower bias, as can be clearly seen in the inset of Figure 4. This is because the longer alkanethiol molecules are less tilted under the same tip-loading force. The longer and more rigid alkyl chains stabilized by van der Waals force interactions can more effectively resist the tip stress, so they are less tilted.[15d,24] Therefore, longer alkanethiol molecules have less electric field (less field emission transport) and less barrier height lowering effect by small contribution of the molecular chain-to-chain transport in the overall conduction in molecular junctions under the same loading force than that of smaller alkanethiol molecules. As a result, the transition voltage V_T occurs at a lower bias as molecular length is decreased (Figure 4). Also, this effect is weak under relatively low tip-loading forces due to the reduction of intermolecular chain-to-chain transport in overall conduction.

Figure 5 depicts the transition voltage V_T (from DT to FN tunneling) for alkanethiol SAMs of different lengths (C8, C10, and C12) under various tip-loading forces (from 50 to 100 nN). In this plot, the average V_T values were determined by taking the statistical average of all V_T values obtained from inflection points of all $\ln(I/V^2)$ versus $1/V$ graphs for C8, C10, and C12 SAMs, and the error values were determined as the standard deviation from statistical measurements. As previously mentioned, the transition voltage, V_T, was observed to shift to a lower bias as the tip-loading force of the CAFM was increased, which is due to the enhancement of field emission by the reduction of barrier height. The transition from DT to field emission also occurs at a lower bias for shorter molecules. The solid lines in Figure 5 are the calculated results based on the MBT model considering intermolecular charge transport, which agree well with the experimentally determined values. The best fits with the model were achieved using $\alpha = 0.72 \pm 0.02$ for C8, C10, and C12, which is consistent with previous studies.[13,16,25] We also found that the difference in V_T values for molecules of different lengths becomes smaller as the tip-loading force is decreased, due to the reduction of intermolecular chain-to-chain transport.

4. Conclusion

In summary, we have studied the effect of molecular configuration on electronic transport in alkyl metal−molecule−metal junctions where the molecular tilt configuration was

(24) (a) Xiao, X.; Hu, J.; Charych, D. H.; Salmeron, M. *Langmuir* **1996**, *12*, 235. (b) Israelachvili, J. *Intermolecular and Surface Forces*; Academic Press: New York, 1992.
(25) Kim, T.-W.; Wang, G.; Lee, H.; Lee, T. *Nanotechnology* **2007**, *18*, 315204.

controlled using the CAFM tip. Our results indicate that the transition voltage, V_T, from direct tunneling to field emission through molecules shifts to a lower bias as the tip-loading force of CAFM is increased (i.e., molecular tilt is increased), and molecular length is decreased under high loading force, which is consistent with the theoretical prediction from the multi-barrier tunneling model while considering intermolecular charge transport.

Acknowledgment. This work was supported by the National Research Laboratory (NRL) Program and the National Core Research Center (NCRC) grant by the Korea Science and Engineering Foundation (KOSEF), and the Program for Integrated Molecular System at GIST. We thank Hyunwook Song for discussion on Figure 3 and Sunghoon Song for SEM image of Figure S1, Supporting Information.

Supporting Information Available: SEM image of CAFM tip (Figure S1), I versus V (Figure S2a), and $\ln(I/V^2)$ versus $1/V$ (Figure S2b) for C8, C10, and C12 under 1 nN tip-loading force; the statistical histograms of $\log(I)$ measured at 1.5 V for C8, C10, and C12 with various tip-loading forces (50−100 nN) (Figure S3); the statistical histograms of transition voltage V_T values for C8, C10, and C12 with various tip-loading forces (50−100 nN) (Figure S4); schematics illustrating the geometry of molecules tilted by the tip-loading force (Figure S5), net force (P_n), contact radius (a), applied pressure (P), contact separation ($d_t - \delta$), and tilt angle (θ) calculated according to the Hertzian mechanics; and spring model for alkanethiols (C8, C10, and C12) at given tip-loading forces (Table S1). This material is available free of charge via the Internet at http://pubs.acs.org.

JA900773H